



Universiteit  
Leiden  
The Netherlands

## Unconventional fabrication of 2D nanostructures and graphene edges

Bellunato, A.

### Citation

Bellunato, A. (2018, December 11). *Unconventional fabrication of 2D nanostructures and graphene edges*. Retrieved from <https://hdl.handle.net/1887/67524>

Version: Not Applicable (or Unknown)

License: [Licence agreement concerning inclusion of doctoral thesis in the Institutional Repository of the University of Leiden](#)

Downloaded from: <https://hdl.handle.net/1887/67524>

**Note:** To cite this publication please use the final published version (if applicable).

Cover Page



Universiteit Leiden



The handle <http://hdl.handle.net/1887/67524> holds various files of this Leiden University dissertation.

**Author:** Bellunato, A.

**Title:** Unconventional fabrication of 2D nanostructures and graphene edges

**Issue Date:** 2018-12-11

# CHAPTER 2

---

## Chemistry at the Edge of Graphene

*The selective functionalization of graphene edges is driven by the chemical reactivity of its carbon atoms. The chemical reactivity of an edge, as an interruption of the honeycomb lattice of graphene, differs from the relative inertness of the basal plane. In fact, the unsaturation of the  $p_z$  orbitals and the break of the  $\pi$  conjugation on an edge increase the energy of the electrons at the edge sites, leading to specific chemical reactivity and electronic properties. Given the relevance of the chemistry at the edges on many aspects of graphene, the present review investigates the processes and mechanisms that drive the chemical functionalization of graphene at the edges. Focus is given to the selective chemical functionalization of graphene edges from theoretical and experimental perspectives, with a particular focus on the characterization tools available to characterize graphene edge chemistry.*

This chapter was published as a review article: Amedeo Bellunato, Hadi Arjmandi Tash, Yanina Cesa and Grégory F. Schneider. Chem. Phys. Chem. 2015, 17(6).

## 2.1 Introduction

Graphene is an allotrope of carbon with a two-dimensional, atomically thin, honeycomb structure<sup>1</sup>. The  $2s$ ,  $2p_x$  and  $2p_y$  orbitals from each carbon atom in the graphene lattice hybridize into three  $sp^2$  orbitals, each developing a  $\sigma$  bond with an adjacent carbon atom. The remaining un-hybridized  $p_z$  orbitals – perpendicular to the graphene lattice – form a conjugated  $\pi$  bond network in which the delocalized electrons are responsible for the electronic properties of graphene, such as a transport velocity only three hundred times lower than the speed of light<sup>2</sup> and the extraordinary high charge carrier mobility<sup>3</sup>.

Breaking the aromaticity of the honeycomb lattice – for example by creating edges – alters the properties of graphene<sup>4</sup> and, depending on the crystallographic orientation of the lattice, two types of edges are observed: zig-zag and armchair edges<sup>5</sup>, each characterized by specific chemical reactivity and electronic properties.

The chemical reactivity of the carbon atoms localized on a graphene edge differs from the relative inertness of the basal plane<sup>6</sup>. Broken  $\sigma$  bonds at the edges develop radical groups with accessible and highly active electrons. The conjugation system is different on a zig-zag edge compared to an armchair edge, yielding significant discrepancies in reactivity<sup>7,8</sup>.

Furthermore, depending on the chemical properties of the group grafted on the edge,  $p$  or  $n$  doping can be promoted, leading to the modulation of the electrical conductivity of graphene. Local defects in the graphene lattice (such as dislocations or imperfections) can also be considered as edges as they define a termination of the conjugated honeycomb network<sup>7,9,10</sup>.

Edges form during the exfoliation of graphene from graphite<sup>11</sup> as well as during the chemical growth of graphene sheets<sup>12</sup>, or as a result of mechanical and chemical processes such as ionic bombardment, and reactive etching of the basal plane, to name a few<sup>13</sup>. Forming a crystalline edge with a predefined orientation (i.e., zig-zag or armchair) is particularly important in order to specifically address the chemical reactivity of graphene. Thus, the ability to distinguish the edge from the basal plane is crucial to characterize the edge. Several techniques are employed to

do so, for example scanning tunnelling microscopy<sup>4,14</sup>, Raman spectroscopy<sup>10,15,16</sup> and high resolution electron microscopy<sup>17–19</sup>.

The presence of edges and defects in graphene promote new possibilities to tailor the chemistry of graphene with additional implications on the physical and electrical properties of graphene. Considering the rapidly growing interests in the field, this review aims to provide an overview over the most appealing topics concerning the edges of graphene and their chemistry.

## 2.2 Chemical reactivity of graphene edges

An edge in graphene forms following the breaking of  $\sigma$  bonds between adjacent carbon atoms and of the  $\pi$  conjugation network. Depending on the orientation of the edge along the honeycomb structure, two configurations arise: namely the zig-zag and the armchair edges (Figure 2.1a). An edge, however, typically does not develop along a unique crystallographic direction and leads to more complex geometries often with alternated zig-zag and armchair segments known as “chiral edge”<sup>20</sup>.

In absence of reactants (i.e. in ideal vacuum), the atoms on the edges are di-radicals observed as metastable  $\sigma$  and  $\pi$  dangling bonds<sup>8,21–23</sup> with unsaturated  $sp^2$  and  $p_z$  orbitals<sup>24</sup>. Dangling bonds can develop during the edge formation. They are unstable and difficult to observe. In fact, for instance, the electrons of an armchair edge could reduce their energy by establishing a triple bond between the outer carbon atoms<sup>24</sup>. On a zig-zag edge, instead, the  $p_z$  electrons are confined on each outer carbon atom and maintain a radical singlet configuration responsible of the so called “edge state”<sup>25–28</sup>, Figure 2.1a. Consequently, zig-zag edges are very energetic and the planar reconstruction of six-fold benzene rings to pentagonal or heptagonal structures often occurs to lower their energy<sup>28</sup>. The atomic structure of the edges determines the presence of specific electronic distributions that affect the energy states of the atoms on the edges and, consequently, their chemistry.

Graphene can be represented as a polycyclic aromatic hydrocarbon (PAH) built by translation of a hexagonal unit cell of benzene ( $C_6H_6$ ). Interestingly, the chemical reactivity of graphene can be expressed from the aromaticity of its PAH representation. For a cyclic hydrocarbon such as benzene, a ring deriving from the overlap of the resonant structures of the molecule and representing the

delocalization of the  $\pi$  electrons between the unsaturated  $sp^2$  carbon atoms best represents the aromaticity. The most stable structure of a PAH molecule is the one maximizing the number of aromatic rings among its unit cells (known as Clar's structure).

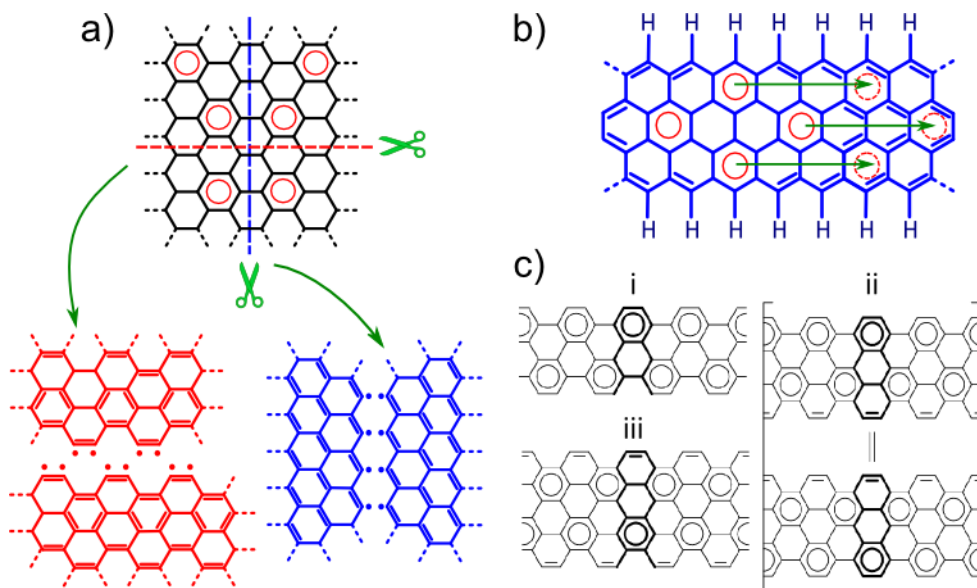


**Figure 2.1.** The edges of graphene. a) Formation of edges in graphene by cutting along the two crystallographic directions: blue) zig-zag edges and the singlet radical bond; red) armchair edges and rearrangement of radicals into triple bonds. b) Chemical structure of a graphene nanoribbon with zig-zag edges. The green arrows depict the isomeric structures obtained by sliding the position of the aromatic rings across the ribbon<sup>29</sup>. c) Armchair graphene ribbons. The number of isomeric structures and the presence of localized double bonds depend on the width  $n$  of the graphene. (i) has a unique isomeric structure, while (iii) has a unique isomeric structure with double bonds localized at the edges. (ii) has localized double bonds on the edges and more than one resonant structure<sup>30</sup>.

Similarly, the aromaticity of the graphene<sup>31</sup>, and particularly its reactivity at the edge can also be defined by the overlap of the different isomeric Clar's structures. Importantly, the edge geometry influences the aromaticity of graphene as shown in Figure 2.1b-c. For a semi-infinite zig-zag ribbon three hexagons wide (Figure 2.1b), the zig-zag geometry promotes infinite isomeric Clar structures, primarily because aromatic rings can slide along the length of the ribbons, highlighting the intrinsic reactivity of the molecule<sup>32</sup>. Independently from their width, zig-zag graphene ribbon can not be represented with a fully benzenoid structure. Thus,

the graphene aromaticity is in balance between the aromatic ring along its lattice and the highly reactive localized double bonds present on the edge. A semi-infinite armchair graphene ribbon, however, shows a limited number of Clar's formulas independently of the width of the structure indicating a lower chemical reactivity (Figure 2.1c). In fact, the width of the ribbon also influences the overall aromaticity of the graphene molecule and therefore its subsequent chemical reactivity. For example, PAH (i) and (iii) have a unique resonant structure regardless of the different width, but while (i) is fully benzenoid with no localized double bonds, (iii) is defined as a Kekule molecule, without a fully benzenoid structure and with reactive double bonds localized on the edges. The molecule (ii), however, can be divided in a fully benzenoid molecule connected to a strip of non-aromatic hexagons with double bonds localized on the edges. The two resonant structures imply two configurations with the double bonds localized on the opposite sides of the molecule (Figure 2.1c, (ii)), revealing a chemical reactivity comprised between a benzenoid system and localized double bonds<sup>30</sup>. In conclusion, the chemical reactivity of the edges of (ii) is expected to be lower than (iii), even in presence of multiple resonant structures. In fact, the edges of (iii) present reactive localized double bonds, while the reactivity of the edges of (ii) is modulated by a resonant structure with an aromaticity extended up to the edges.

The difference between zig-zag and armchair graphene nanostructures is therefore that zig-zag edged molecules are incompatible with a fully benzenoid graphene molecule and are expected to present localized double bonds. For armchair graphene molecules, however, the reactivity is modulated by the probability of having either an aromatic ring or localized double bonds on its edges.

The Clar's representation of graphene is therefore a simple and effective method to link the edge configuration with the reactivity of a particular graphene molecule. The specific reactivity of the edges is modulated by the probability of finding a localized double bond at the edge.

In most PAH representations, molecules are mono-hydrogenated at the edge. To what extent does the aromaticity and/or the edge structure impact the reactivity of that particular C-H is still poorly understood for graphene. Thermodynamics say that the conversion of C-H into a functional group is determined by the variation of the free energy of the system upon functionalization, which requires to consider

external factors such as the chemical activity of the functional group and the specific chemistry of the carbon atoms in proximity<sup>33</sup>. So, in chemically complex environments it is difficult to foresee the specific chemical functionalization of the edges at the atomic scale, because of the many possible combinations that can satisfy the thermodynamic criteria of the functionalization<sup>34</sup>. Nevertheless, simple systems like graphene exposed to H<sub>2</sub> have been modelled. Thermodynamically, the hydrogenation of the edges is driven by the chemical potential of the molecular hydrogen,  $\mu_{\text{H}_2}$  and the energy of the system tends to decrease with a higher density of hydrogen functionalities on the edges. Consequently, at standard conditions of pressure and temperature, zig-zag graphene tends to acquire a particular configuration known as ZZ(211), Figure 2.2a. Practically, it leads to a semi-benzenoid configuration which limits the amount of double bonds on the edges, according to the corresponding Clar representation<sup>29</sup>.

In conclusion, Clar's structures represent well the break of the lattice symmetry induced by an edge according to the probability of finding a localized double bond. Tuning precisely the geometry and the specific chemistry of an edge in formation is, however, still a difficult exercise in practice.

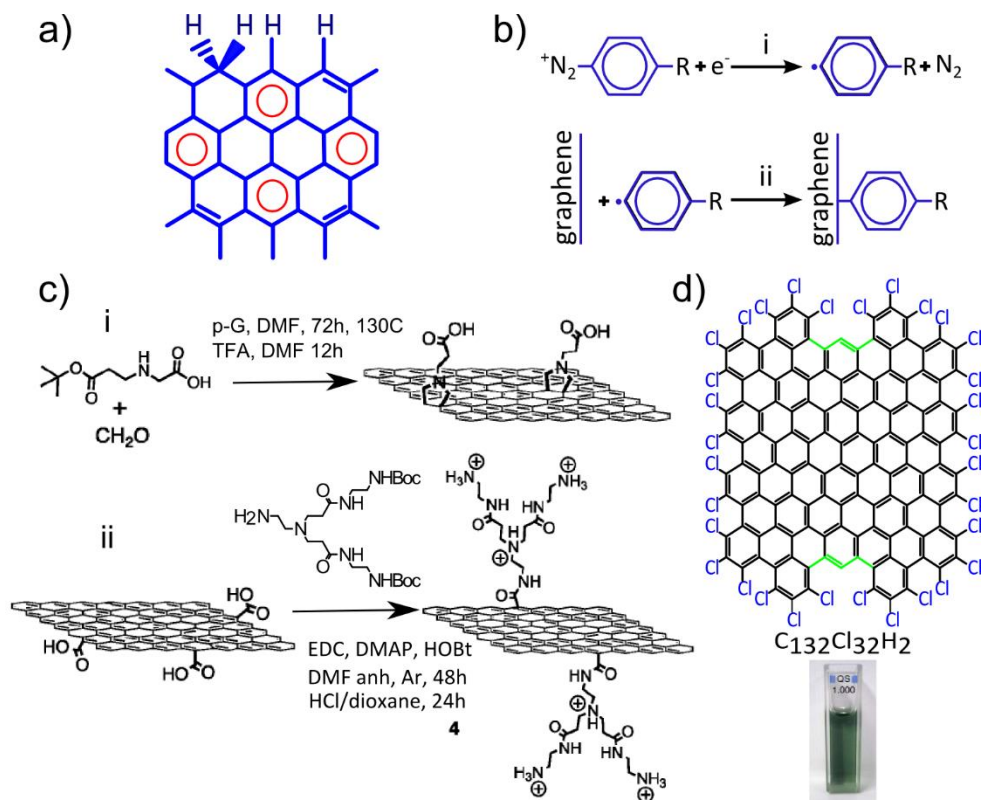


**Figure 2.2.** Functionalized edges. a) zz(2,1,1) edge configuration of a zig-zag edge. b) Chemical reaction scheme of an aryl-diazonium salt onto graphene<sup>35</sup>. The reaction proceeds in two steps: the electrophilic salt dissociates to form  $\text{N}_2$  and an aryl radical (i). The reactive aryl radical binds the nucleophilic graphene (ii). c) (i) Scheme of cycloaddition on exfoliated graphene (p-G) of a molecule of paraformaldehyde conjugated with a modified alpha amino acid. (ii) Direct condensation of the dendron on the carboxyl functionalities on the edge of the pristine exfoliated graphene<sup>36</sup>. d) Top, Edge chlorination of nanographene (PAH systems). The functionalization is influenced by the topography of the molecule, gulf regions are not functionalized because of steric hindrance effects<sup>37</sup>. Bottom, edge chlorinated graphene dispersion in toluene.

### 2.3 Chemical functionalization of graphene edges

Organic chemistry allows the design of peculiar edge terminations that are known to modulate the physical properties of graphene without severely altering the aromatic structure of the basal plane<sup>38</sup>. While edge functionalization has primarily been investigated in liquid-based exfoliation procedures, recent electron beam

methods yielding crystalline graphene edges suggest new research routes to selectively functionalize graphene edges.

### 2.3.1 Liquid-based functionalization of graphene edges

Two main approaches were proposed to achieve the selective functionalization of graphene edges in solution. In a first approach, edge functionalized graphene flakes were fabricated by exfoliating graphite using organic reactions such as diazonium electrografting, 1-3 dipolar cyclo-addition and Friedel-Crafts acylation, which are well known organic reactions used to functionalize graphene<sup>39</sup>. For example, the acylation of graphite using poly (phosphoric acid) (PPA) and phosphorous pentoxide ( $P_2O_5$ ) in presence of 4-aminobenzoic acid resulted in 4-amino-benzoyl-functionalized graphite<sup>40</sup>. The acylation typically proceeds through electrophilic substitution at the  $sp^2$  C-H atoms located mainly at the edges<sup>41</sup>. The acylation mechanism was modelled using a pyrene molecule treated in PPA/ $P_2O_5$  with 4-(2,4,6-trimethylphenoxy)benzamide (TMPBA). The yield of reaction and the amount of edge functionalization was determined by the number of  $sp^2$  C-H sites available for the chemical reaction, and was further improved by the formation/activation of new edges by, for example, ball milling<sup>42</sup> (i.e. the bombardment of graphite with steel balls). Ball milling mechanically breaks C-C bonds within graphite layers, producing unsaturated graphene flakes with highly reactive edges<sup>43</sup>. By subsequently exposing the just formed edges to several reactive gas yielded various functionalizations of the edges. Hydrogen, sulphur, carboxylic acid and other functionalities have therefore been conjugated to the graphene edges, particularly to promote a better solubility of graphene flakes in organic solvents<sup>43,44</sup>.

Similarly, diazonium chemistry on the edges of graphite was performed in order to produce highly soluble graphene dispersions<sup>45</sup>, Figure 2.2b. The functionalization was obtained by the in-situ reaction of graphite with 4-bromophenyl radicals deriving from the dissociation of the diazonium salt in solution. The selective edge functionalization is ensured by the molecular size of the functional groups grafted at the edges. In fact, 4-bromophenyl is a bulky molecule that hardly intercalates in between graphitic layers. The functionalized graphite was then sonicated in order to exfoliate edge functionalized graphene flakes and to form a stable dispersion in DMF, achieving a solubility in the order of 10-20  $\mu\text{g/mL}$ , with 70% of the flakes

thinner than five layers<sup>45</sup>. The diazo-chemistry has also been widely used to functionalize various other carbon allotropes such as glassy carbon<sup>46</sup> and highly oriented pyrolytic graphite.<sup>47</sup> Additionally, the reactivity of graphene edges with diazonium compounds has been probed and demonstrated to be higher than the one of the basal plane. In fact, the aryl functionalization by diazonium-salt reaction is based on the electron exchange reaction between the nucleophilic graphene and the electrophilic aryl radical forming upon  $N_2$  dissociation. The reaction leads to the covalent functionalization and rehybridization of the edge carbon atoms from  $sp^2$  to  $sp^3$ . In principle the reaction occurs when the density of states of the graphene overlaps the unoccupied electronic states of the aryl radical. Edges are therefore prone to be more reactive than the basal plane. Experimentally, the larger reactivity of the edges vs the basal plane towards diazonium salts has been proven by Raman spectroscopy and transport measurements<sup>48,49</sup>.

A second approach involves the chemical functionalization of graphene flakes already exfoliated in solution. For example, 1,3 dipolar-cycloaddition in combination with amide-bond condensation was carried in order to probe whether edges are more sensitive to functionalization<sup>36</sup>. Two reaction schemes were proposed. First, paraformaldehyde conjugated with a modified alpha amino acid undergoes a cycloaddition reaction with graphene. The functionalized graphene was then subjected to a condensation reaction with an aminated dendron such as the one shown in Figure 2.2c (i). In a second case, pristine graphene was directly subjected to a condensation reaction with the dendron (Figure 2.2c (ii)), directly reacting with the carboxylic acid functionalities on the edges formed during the exfoliation process<sup>50</sup>. It has been reported that the condensation after cycloaddition yielded a functionalization degree five times higher than the direct condensation on the carboxylic groups. In fact, the cycloaddition lacks the edge selectivity and offers docking sites for the condensation reaction to happen on the edges and on the basal plane. The direct condensation on the carboxylic groups, instead, is constrained on the edges, since the carboxylic functionality develops only (almost) on the edges during the exfoliation<sup>50</sup>.

Selective edge functionalization was also carried on chemically synthesized nano-graphene flakes<sup>51</sup>. PAH systems of different size and topography were chlorinated in  $CCl_4$  at 80 °C with  $AlCl_3$  as a catalyst<sup>37</sup>. The edge selectivity was obtained using

electrophilic substitution reactions only occurring with  $sp^2$  C-H which are only present on the edges. Interestingly, the reaction yield is largely influenced by gulf regions which cannot be functionalized because of steric hindrance effects (Figure 2.2d, in green).

### 2.3.2 Direct beam lithography: chemical perspectives

Direct beam lithography uses highly focused electrons (above 80 keV) or ions (typically helium or gallium above 30 keV) to form edges by knocking out carbon atoms from the lattice or by breaking C-C bonds<sup>52,53</sup>. The absence of lithographic resists preserves the edges from contaminations, making direct beam lithography particularly suitable to control the chemical structure of the edges and their post functionalization<sup>54,55</sup>.

So far, research focused on forming graphene nanoribbons primarily with the goal of opening a band-gap. Importantly, the control over the crystallinity of the resulting edges (i.e., zig-zag vs. armchair), showed a large impact on the electrical properties of ribbons, e.g. from being semi-conducting to metallic<sup>56,57</sup>. Adding electron donating or withdrawing group at the edge result in different doping levels<sup>58</sup>.

Graphene edges are typically fabricated by lithography, using transmission electron microscopes (TEM) or focused ions beams (FIB)<sup>55,59–65</sup>. TEM sculpting at temperature up to 700°C yields graphene nanostructures which remain crystalline up to the edges, also preserving the graphene from contaminations and amorphization<sup>66</sup>. The absence of amorphization and defects at high temperatures suggests the presence of a self-repair mechanism, where the carbon ad-atoms (either knocked out from the lattice or originating from carbon-rich contaminations) migrate on the surface and heal the defect sites in the graphene crystal, Figure 2.3a.

The technique was further improved in the scanning transmission electron microscopy (STEM) mode of the TEM<sup>54</sup>, where the beam of electrons is focused onto a sharp spot ( $d \sim 1 \text{ \AA}$ , less than an atom size) whose position is controlled with sub-nanometric precision, Figure 2.3b. High-temperature STEM is a very unique technique for sculpting graphene, atom-by-atom, and to customize the orientation of edges into zig-zag or armchair configurations.

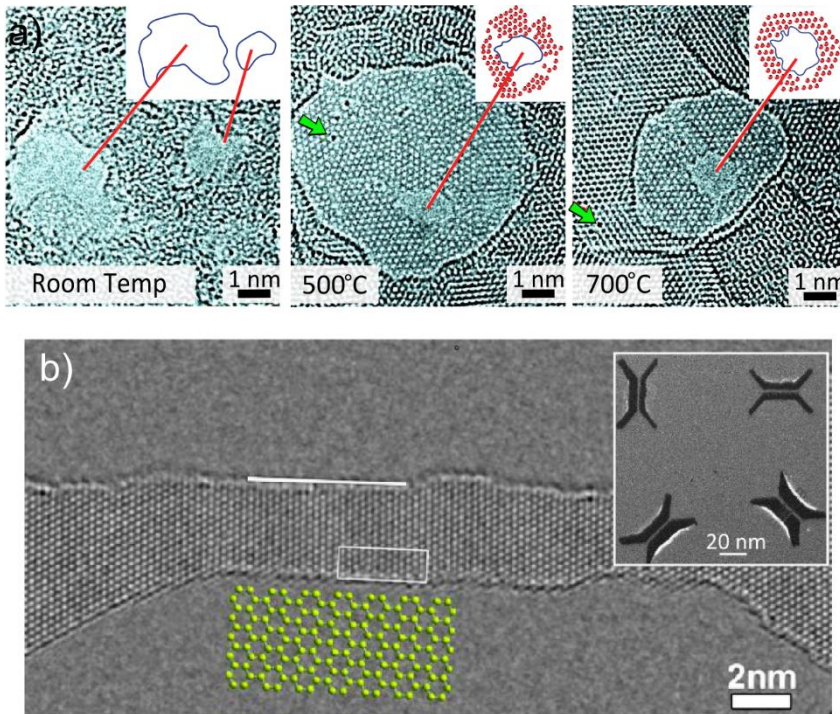


**Figure 2.3.** Direct beam lithography of graphene edges. a) High resolution transmission electron micrographs of few-layer graphene sculpted in the bright-field mode of a transmission electron microscope (TEM) at different specimen temperatures<sup>66</sup>. The estimated positions of the identifiable hexagons and location of the carbon atoms at the edge are represented by red dots and blue lines respectively (insets). The green arrows point out carbon ad-atoms trapped at defect sites. b) High resolution TEM micrographs of graphene nanoribbons sculpted by scanning transmission electron microscopy (STEM) at 600°C under a 300 kV electron beam (inset) and imaged at 80 kV<sup>54</sup>. Inset: sculpting of very narrow and similar rotated nanoribbons (inset) highlights the reproducibility of the high temperature STEM sculpting process.

Similarly to electrons, helium ions were also used to create edges in graphene<sup>67</sup>. The minor interaction of helium ions with graphene allowed the reduction of the beam size down to  $\sim 2.5 \text{ \AA}$ <sup>68</sup>, a value comparable – but still larger – than the STEM sculpting technique<sup>54</sup>.

### 2.3.3 Reactive plasma etching

Lithographic techniques are typically used in combination with reactive plasma to pattern edge-like structures in graphene<sup>13</sup>. The highly energetic ions and radicals

inside a plasma can interact mechanically and/or chemically with graphene. Plasma etching is a chemical reaction between the species in the plasma and the carbon atoms of the graphene, which preferentially starts from the chemically active sites on graphene, such as edges and defects<sup>69,70</sup>.

Etching of graphene in presence of a H<sub>2</sub> plasma showed that the hydrogenation of the graphene preferentially occurs at the edges forming mono-hydrogenated and di-hydrogenated edges<sup>71,72</sup>, while developing volatile CH<sub>4</sub> and preserving the integrity of the basal plane<sup>69</sup>. The thermodynamic stability of mono-hydrogenated and di-hydrogenated edges depends on the chemical activity of hydrogen. The chemical potential  $\mu_{\text{CH}}$  and  $\mu_{\text{CH}_2}$  varies with temperature and pressure: mono-hydrogenated edges preferably form at standard conditions of T=300 K and low H<sub>2</sub> pressure (e.g. in air with a H<sub>2</sub> partial pressure in the order of 10<sup>-4</sup> mbar)<sup>73,74</sup>, while di-hydrogenation occurs at higher H<sub>2</sub> pressure and results in a sp<sup>3</sup> re-hybridization fully saturating the carbon orbitals and requiring the arrangement of the hydrogen functionalities out of the graphene plane, increasing the CH<sub>2</sub> configuration energy<sup>75</sup>. The amount of mono-hydrogenated vs. di-hydrogenated edges varies and is proportional to the thermodynamic stability of graphene in presence of H<sub>2</sub>, and depends on the activity of the gas (i.e. the partial pressure of the gas and the temperature). Consequently, it was shown that the amount of CH<sub>2</sub> terminated edges rises proportionally with the hydrogen partial pressure at a given temperature<sup>74</sup>.

Similarly, in presence of O<sub>2</sub>, graphene edges get oxidized. Theory predicts that ketones and ethers are the most stable configurations<sup>56</sup>. The principal difference between ketones and ethers lays in the bond structure with the carbon atoms. The ketones maintain the sp<sup>2</sup> hybridization of the carbon atoms. The ether groups, instead, bind two carbon atoms and develop a planar configuration on both the armchair and zig-zag edges<sup>56,76</sup>. Similarly to the case of hydrogenation, the oxidation is driven by the chemical activity of the O<sub>2</sub> and the structural configuration of zig-zag or armchair edges<sup>34</sup>. The oxidation of the edges appears to lower the free energy of the system by maximizing the density of oxygen groups per carbon atoms, yielding to CO<sub>2</sub> formation, Figure 2.4a (i). Oxygenated edges most likely assume two configurations known as arm-chair O(11) and zig-zag O(11), Figure 2.4a (ii) and (iii), where each carbon atom on the edge. Zig-zag edges are prone to form cyclic ester at the edges by esterification of carboxylic groups. The

process has a negative energy of formation and has been used to electrochemically functionalize edges<sup>34,77,78</sup>.

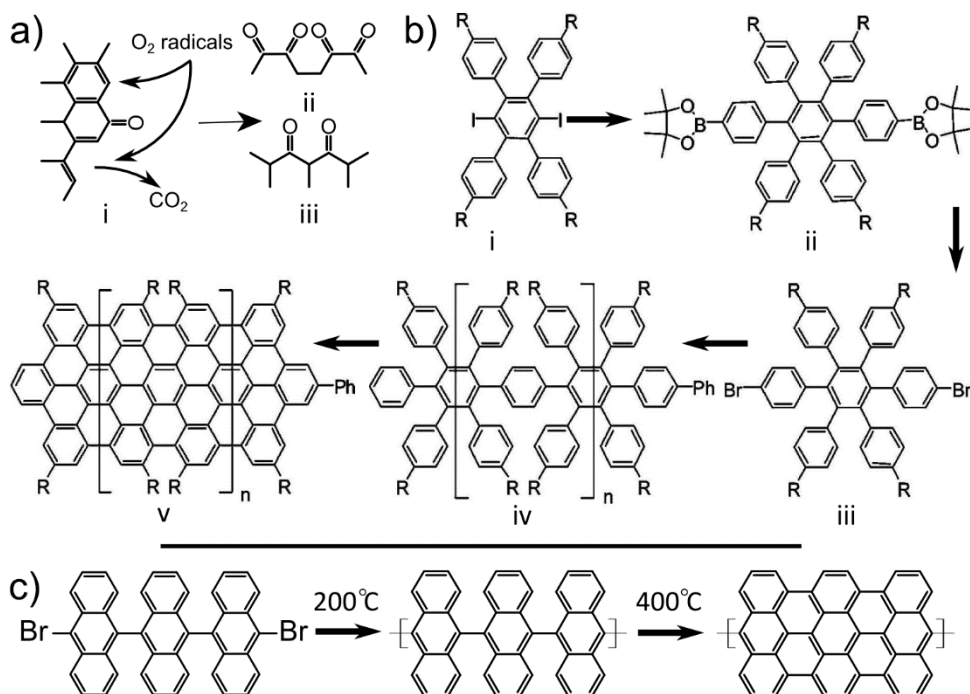


**Figure 2.4.** Design and functionalization of graphene edges. a) (i) Etching and functionalization of graphene in  $O_2$  plasma. (ii) and (iii) are the preferential functionalization configurations in presence of  $O_2$  at equilibrium with the formation of  $CO_2$ <sup>34</sup>. b) Solution synthesis of graphene nanoribbons from a 1,4 tetraphenylbenzene precursor in solution<sup>79</sup>. c) Surface assisted synthesis of graphene nanoribbons from a bianthryl monomeric precursor<sup>80</sup>.

Among the factors that influence the functionalization mechanisms, the steric hindrance of the functional groups or the development of a mechanical stress state can influence the functionalization. For example, theoretical models foresee hydroxyl functionality to be even more stable than oxidized or hydrogenated edges<sup>78</sup>, even if  $-OH$  groups develop out of plane functionalities, which could lead to stress states on the graphene.

Another important edge passivation mechanism is the amination. The nitrogen chemistry is particularly interesting in some research fields such as molecular sensing<sup>81</sup>. Under standard conditions it is difficult to predict the most stable

configuration. In the simplest model, aromatic zig-zag edges exposed to ammonia tend to acquire specific configurations, consisting of an NH group every two mono-hydrogenated carbons. Armchair edges, instead, most likely alternate mono-hydrogenated carbons and NH<sub>2</sub> functionalities<sup>34</sup>. Thermodynamically, these configurations are the most stable, but the break of the NH<sub>3</sub> molecules in plasma can lead to the formation of other energetic radicals competing with the NH<sub>2</sub> functionalization (i.e., N°, NH°, and H° radicals). It is thus complicated to assume a unique functionalization of the edges with a single species in presence of an ammonia plasma<sup>81–83</sup>. Experimentally, the application of a mild NH<sub>3</sub> plasma yielded the functionalization of graphene edges with nitrogen atoms. With a 25 W NH<sub>3</sub> plasma, chemical reactions were also specifically promoted at the edge preserving the basal plane<sup>83</sup>. Additionally, the reactivity of the edges with ammonia, has been studied following the *n*-doping of graphene nanoribbons in presence of a NH<sub>3</sub> plasma<sup>81</sup>. Amination has been also achieved in presence of NH<sub>3</sub> exploiting the self-heating of graphene upon electron beam irradiation. The self-heating excites the graphene atoms and provides the energy for the functionalization reactions<sup>82</sup>.

Reactions of graphene edges in plasmas are governed by several parameters such as the gas mixture, the partial pressure and the temperature<sup>69</sup>, which tune the reactivity of both the plasma species and the graphene. For example, low temperature stimulates the recombination of the reactive species into molecules before reaching the graphene surface, reducing the supply of reactants. Elevated temperatures, instead, provoke a strong increase of the basal plane reactivity, yielding more uncontrollable reaction rates and the loss of the edge selectivity<sup>69</sup>. Similarly, the pressure as well as the power of the plasma influence the energy of the ions and radicals reaching the graphene, promoting or limiting the reaction rate and the edge selectivity.

### 2.3.4 Organic synthesis of functional graphene edges

The chemical synthesis (also known as “bottom-up”) of nanographene via the polymerization of molecular building blocks of aromatic molecules is among the most powerful methodologies to fabricate functional graphene edges<sup>79</sup>. Graphene ribbons with length up to 12 nm (Figure 2.4b) were synthesized using this method, particularly using the reaction of 1,4 tetraphenylbenzene (**i**) with bromophenylboronic acid yielding a hexaphenylbenzene derivative (**ii**). In a second

step, **(ii)** reacts with n-butyllithium and 2-isopropoxy-4,4,5,5-tetramethyl-[1,3,2]dioxaborolane to form compound **(iii)** that subsequently polymerizes producing polyphenylene **(iv)**<sup>79</sup>. The resulting polyphenylene undergoes a graphenization reaction<sup>51</sup> through de-hydrogenation, forming compound **(v)**, which is a precursor of graphene. Several routes exist to strip off the hydrogens from the precursor. One approach is the FeCl<sub>3</sub>-Scholl mediated reaction<sup>51,79</sup> which yields graphene nanoribbons of up to 100 nm in length<sup>84</sup>. The functional groups R used on the outer phenyls are generally alkyl chains. In fact, long aliphatic chains reduce the aggregation tendency of the polymer (i.e. the polymerized ribbon) by preventing intermolecular  $\pi$ -stacking, promoting its solubility. The molecular size of the graphene precursor is crucial, as larger precursors tend to be less soluble, yielding aggregation and precipitation even before the polymerization starts<sup>51,79,84</sup>.

To overcome the aggregation tendency of the graphene in solution, surface thermal assisted polymerization has been developed<sup>80</sup>. The synthesis involves the adsorption of a bianthryl monomeric precursor on a metallic surface, usually Au(111), which topography and grain boundaries determine the size of the obtained graphene ribbons<sup>51,80</sup>. Next, a thermal annealing induces the di-radicalization of the monomer and provides the driving force for the surface diffusion of precursors leading to the polymerization. After this step, the polymer is still hydrogenated, hence the requirement for a further thermal annealing step which activates the intra-molecular cyclo-dehydrogenation and the planarization of the molecule into sp<sup>2</sup>-bonded nanographene (Figure 2.4c). The drawback, however, is that the surface-assisted synthesis is dependent on the quality of its processing environment: it requires ultra-high vacuum (UHV) to avoid any contamination that could prominently react with the graphene in formation, hence also degrading its edges<sup>80</sup>.

Using bottom-up approaches, the topology of the synthetic graphene is fully governed by the chemical structure of its precursor, allowing the synthesis of atomically precise graphene structures, more particularly graphene with tunable edge chemistry and geometry, which is a unique feature of the bottom-up chemical synthesis. The chemical synthesis of graphene also faces the important issue concerning the achievable size of graphene which do not yet reach the dimension obtained by mechanical exfoliation<sup>1</sup> or chemical vapor deposition<sup>85</sup>.

### 2.3.5 Functionalization of graphene edges by anodic oxidation

Scanning tunnelling microscopy (STM) and atomic force microscopy (AFM) are the typical scanning probe microscopes employed in anodic oxidative lithography<sup>86</sup>.

The probe (or tip) is driven over graphene in proximity of its surface. The adsorbates on the surface build a meniscus that connects the surface to the tip, providing the reactants for the anodic oxidation. The potential difference applied between the surface and the tip ignites the reaction, etching the carbon atoms of graphene and producing functional edges and volatile compounds such as CO and CO<sub>2</sub><sup>87-90</sup>.

The anodic oxidation is electrochemically driven and depends on the applied bias voltage, the tip velocity, the distance between the tip and the graphene and the relative humidity in the air<sup>91</sup>. More precisely, STM lithography operates via tunnelling current. On a flat surface such as graphene, the tunnelling current selectively flows through the atomic features at the very top of the probe, constraining the oxidation into a narrow conductive channel on the surface of graphene and promoting the nanometric resolution<sup>86</sup>.

AFM lithography, instead, operates without tunnelling current: the applied bias distributes from the tip to the graphene through the meniscus<sup>92,93</sup>. The size of the conductive channel is comparable to the size of the meniscus on the tip. As a result, AFM lithography typically achieves edges with a resolution in the order of 10-15 nm<sup>94</sup>.

From a chemical point of view the control over the chemistry of the edge is rather complex. There is a lack of literature about the chemical composition of fresh cut edges. Incomplete oxidation processes yield graphene oxides on both the surface and the edges of graphene, particularly if the field intensity is weaker than the threshold required for the complete carbon oxidation<sup>95</sup>.

Anodic oxidation of graphene develops carbon oxides on the patterned edges, which is generally considered as a drawback of this technique, while it can be a valuable tool to control the chemistry of the edges, especially in the perspective of post-functionalization.

## 2.4 Electrochemistry of graphene edges

The perturbation of the conjugation system increases the local density of states at the edges and at defects sites<sup>96,97</sup>. Thus, the electrochemical activity of an graphene edge is expected to be higher than the basal plane<sup>8</sup>. In fact, cyclic voltammograms of graphene edges show an electron transfer current up to four orders of magnitude higher than the basal plane (Figure 2.5 a,b). The square shape of the curves highlights the capacitive behaviour of graphene, with a capacitance at the edges estimated to be around  $10^5 \mu\text{F}/\text{cm}^2$  in a 100 mM phosphate buffer supplemented with 100 mM KCl, and reaching a static current density around  $0.1 \text{ A}/\text{cm}^2$  in presence of 5 mM  $\text{K}_3\text{Fe}(\text{CN})_6$  as an electrochemical probe<sup>98</sup>. The stronger electrochemical activity of graphene edges has also been reported in a nanopore device. For that, the graphene sheet was embedded between two insulating  $\text{Al}_2\text{O}_3$  layers<sup>99</sup>, Figure 2.5c. The contour length of the rim of a 5 nm diameter pore (i.e. around 30 nm) yielded an electrochemical current density higher than  $12000 \text{ A}/\text{cm}^2$  in 1M KCl, a value more than four orders of magnitude higher than the previous experiment<sup>98</sup>. This has been attributed to a higher concentration of electrolyte in the solution, in combination with a more prominent convergent diffusion regime promoted by the smaller edge electrode surface<sup>98,99</sup>. In fact, large area electrodes (such as the surface of the graphene) operate in a regime of linear diffusion: the electrolyte approaches the electrode following a linear distribution of the molecules. Contrarily, the convergent diffusion regime strongly depends on the size of the electrode (i.e. the length of the edge), increasing the density of the electrolyte and rising the current density<sup>98-100</sup>.

The higher electrochemical activity of graphene edges with respect to the basal plane has been the starting point for the development of a new class of redox electrodes alternative to the more conventional glassy carbon or graphite electrodes<sup>100,101</sup>. For example, the growth of multilayer graphene platelets lead to the formation of graphene nano-walls with preferential vertical orientation of the platelets, therefore presenting edges facing out perpendicularly to the substrate<sup>102</sup>, and promoting electrochemical reactions specifically at the edges.

As graphene edges yield a more intense electrochemical current, they were used to oxidize dopamine, uric acid and ascorbic acid with a sensitivity sufficient to resolve, by means of CV curves, the separate oxidation peaks of the three

molecules, even when mixed together in a ternary mixture (i.e. 1 mM ascorbic acid, 0.1 mM dopamine and 0.1 mM uric acid, Figure 2.5d)<sup>102</sup>.

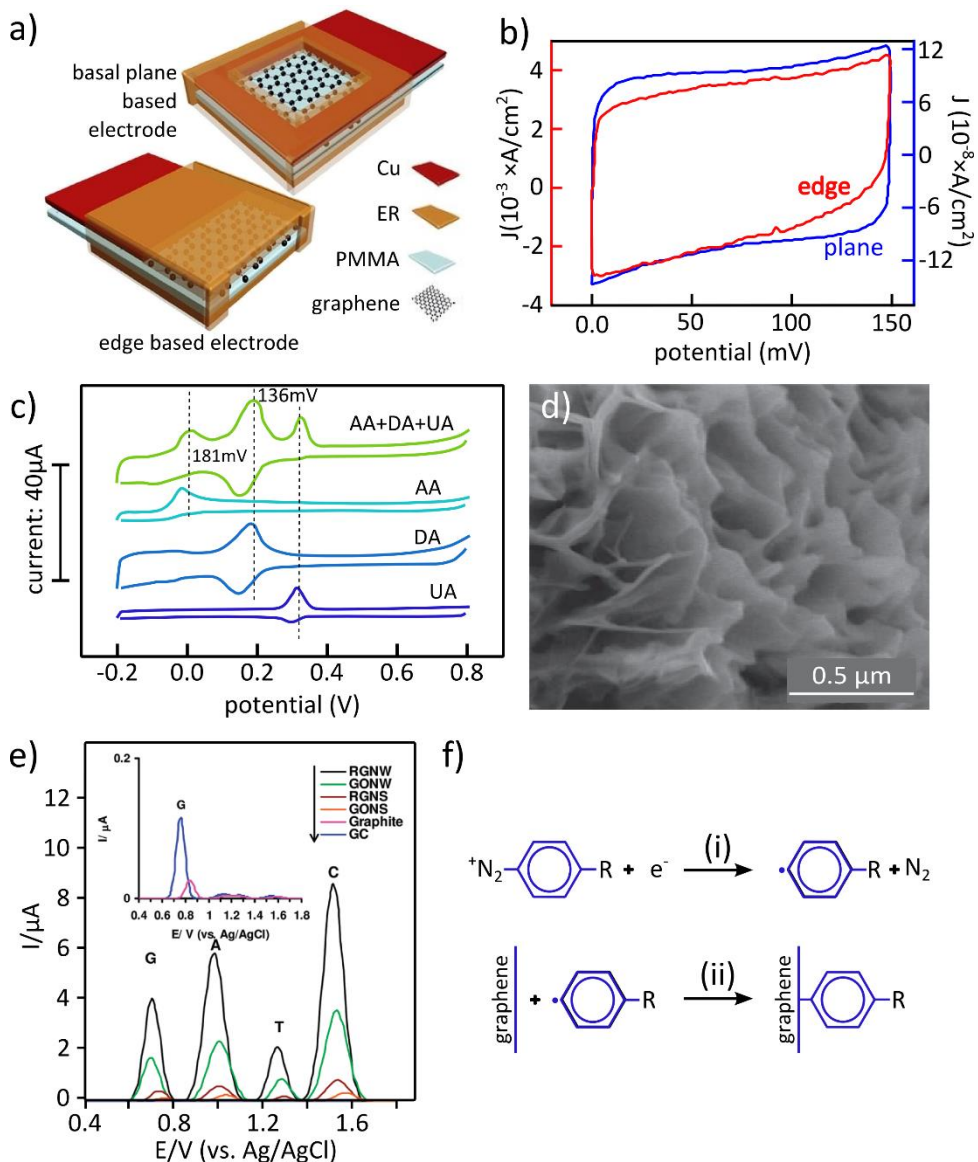


**Figure 2.5.** Electrochemistry of graphene edges. a) Illustration of two graphene electrodes employing respectively the basal plane (top) and the edge (bottom) of graphene. The basal plane electrode has been prepared by embedding the graphene inside a polymeric matrix

and by further etching the coating to solely expose the basal plane. The edge electrode has been prepared by mechanical cutting of the polymeric matrix embedding the graphene leaving only the edge exposed at the cut<sup>98</sup>. b) Cyclic voltammograms (CV) of the basal plane (blue) and of a graphene edge (red) in an aqueous solution of phosphate buffer saline<sup>98</sup>. c) Graphene edge electrode in a nanopore. The graphene is embedded between two Al<sub>2</sub>O<sub>3</sub> insulating layers in order to inhibit the electrochemistry at the basal plane<sup>99</sup>. d) Cyclic voltammograms (CV) of graphene nanowalls (GNW). From top to bottom: solution of ascorbic acid (AA), dopamine (DA) and uric acid (UA). The upper curve is the CV of mixed solution of AA, DA and UA<sup>102</sup>. e) SEM picture of reduced graphene oxide nanowalls (RGNW) electrophoretically deposited on a graphite electrode<sup>103</sup>. f) Comparison between the sensitivity of electrodes made from reduced graphene oxide nanowalls (RGNW), graphene oxide nanowalls (GONW), reduced graphene nanosheets (RGNS), graphene oxide nanosheets (GONS), graphite and glassy carbon (GC) in the detection of the oxidation potentials of the four DNA nucleotides guanine, adenine, thymine, and cytosine (0.1 μM in 0.1 M of PBS, pH=7). The inset is a magnification of the peaks detected by graphite and glassy carbon electrodes which have a much lower detection limit than graphene-based electrodes<sup>103</sup>.

Furthermore, the adoption of alternative production techniques of graphene, such as the reduction of graphene oxide, promoted the rise of defects and residual functionalities<sup>104</sup>, which reduces the quality of the graphene with respect to chemical vapor deposition or exfoliated graphene, but inherently increasing the local electrochemical activity of graphene. Recently, reduced graphene oxide nano-walls electrodes (Figure 2.5e) have been fabricated through the electrophoretic deposition of graphene oxide on top of a graphitic substrate. Its chemical reduction in hydrazine showed that the edges and the surface defects of reduced graphene oxide allowed to detect both single-stranded and double stranded DNA molecules with an improved sensitivity compared to more conventional carbon electrodes such as graphite and glassy carbon<sup>103</sup>. The results, when compared to graphene oxide electrodes (i.e. before the reduction), highlighted the efficiency of the reduction step in increasing the sensitivity towards resolving between the four nucleotides (Figure 2.5f). The higher sensitivity (at least with respect to graphene oxide) has been ascribed to the higher availability of electrochemically active sites on the reduced graphene oxide, consequence of the presence of graphene edges whose aromaticity is shared with the conducting basal plane of graphene (note that graphene oxide is an insulating material). Interestingly, it was observed that the signal resulting from single stranded DNA is higher than for double stranded DNA, explained by the fact that double stranded

DNA has a higher resistance toward oxidation<sup>103,105</sup>, perhaps thanks to the fact that in double-stranded DNA nucleotides are buried within the interior of the  $\alpha$ -helix.

The concentration of analyte can be a limit in the sensing performance of a graphene edge. Nevertheless, in the case of DNA nucleotides, the strong electrochemical behaviour of reduced graphene oxide exploits the high sensitivity of the graphene edges to push the detection limits to concentrations down to 0.1 fM. The upper limit instead was confirmed to be below 10 mM, as a result of the aggregation tendency of the DNA molecules on the graphene surface, which decreases the electrodes activity<sup>103,105</sup>.

## **2.5 Characterizing the chemical functionality of a graphene edge.**

Several techniques have been employed to characterize the structure, topography, chemical functionalities, and electronic properties of graphene. Nevertheless, it is still a challenge to distinguish the chemical composition and the atomic structure of the edges with respect to the basal plane, primarily because the number of carbon atoms located on the edges only represents a small fraction of the total carbon atoms constituting graphene. Just a few methods allow such differentiation being even sensitive to the chemical functionality of the edge.

### **2.5.1 Scanning tunnelling microscopy, STM**

Scanning tunnelling microscopy (STM) can effectively resolve between the edge and the basal plane of graphene, providing atomic resolution imaging of the edges.

Under an applied bias voltage, the electrons tunnel between the STM tip and the surface of graphene, Figure 2.6a. The distance between the tip and the surface of graphene, the applied bias voltage, as well as the intensity of the tunnelling current, are used to extract information about the surface of the sample (e.g. topography, defects and density of charge carriers). Remarkably, the localization of the  $p_z$  electrons on the zig-zag edges of graphene (the “edge state”) locally increases the tunnelling current: the zig-zag edges are visible as brighter spots in STM micrographs, Figure 2.6b (top). These edge states can be further investigated in the scanning tunnelling spectroscopy (STS) mode of the STM. STS measures the first derivative of the tunnelling current with respect to voltage, i.e.  $dI/dV$ ,

revealing the density of the charge carriers at a specific point<sup>4,106,107</sup>, Figure 2.6b (bottom).

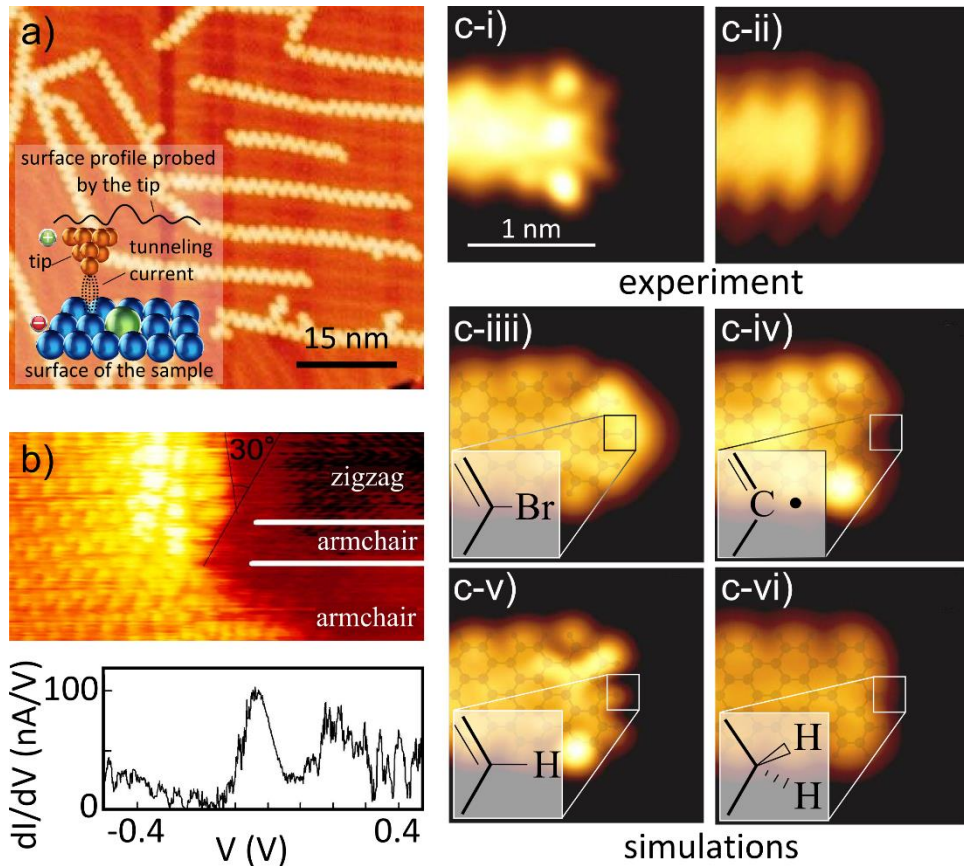


**Figure 2.6.** Scanning tunnelling microscopy of graphene. a) Scanning tunnelling microscopy (STM) imaging of graphene nanoribbons produced by surface assisted chemical synthesis of graphene on a gold substrate<sup>80</sup>. The inset illustrates the working principles of a STM. b) Top: STM mapping of an edge presenting zig-zag and armchair segments, the brighter spots correspond to the higher local charge carrier density of the zig-zag segment, which is absent along armchair sections. Bottom: plot of the tunnelling current derivative against the tip voltage (i.e.  $dI/dV$ ). The more intense peak corresponds to one of the brighter zig-zag edges imaged in the mapping on top<sup>72</sup>. c) Impact of the edge chemical functionality on STM micrographs. (i) and (ii) experimental STM micrographs of chemically synthesized graphene nanoribbons with two presumably unknown termini. (iii) to (vi): density functional theory (DFT) simulations of the STM images for graphene nanoribbons terminated with four different functional groups (The inset represents the chemical structure of the graphene termini)<sup>14</sup>.

STM measurements combined with theoretical calculations allowed to identify the chemical composition of the graphene edges<sup>17</sup>. STM imaging (Figure 2.6c (i-ii)) of chemically synthesized graphene nanoribbons with unknown chemical terminations were compared to the simulated electronic structures of four ribbons with different chemical termini: Br, mono- and di-hydrogenated as well as radical carbon terminations (Figure 2.6c (iii-iv)). Hydrogen passivated carbons show the best matching, highlighting that mono- and di-hydrogenated edges are the most notable termini (Figure 2.6c (v and vi)). Remarkably, most of the ribbons measured experimentally in this work (85% of the total) showed mono-hydrogenated terminations<sup>14</sup>.

To further investigate the effect of the edge hydrogenation on the electronic structure of graphene, nanoholes with predominantly zig-zag hydrogenated edges were fabricated using low energy argon ion bombardment of a graphitic surface, immediately followed by hydrogen plasma etching<sup>73</sup>. The STM micrographs, when compared to simulations, showed that hydrogenating the zig-zag edges distorted the distribution of the electronic structure: while for mono-hydrogenated carbon edges the local charge densities were stretched towards the centre: they were parallel to the edges if di-hydrogenation occurs. In other studies, surprisingly, zig-zag terminated graphene did not show the existence of the localized edge states (i.e. absence of bright spots in the STM images). Density functional theory (DFT) calculation and thermodynamic stability analysis showed that the absence of the edge state occurs when every third edge sites (not all of the carbon atoms) are di-hydrogenated (Figure 2.7d)<sup>73</sup>. The presence of localized edge states on zig-zag edges (Figure 2.7 a,c), which are absent on armchair edges, are the most appealing distinctions between zig-zag and armchair edges in STM. Additionally, in a particular configuration zig-zag edges do not show the edge state (Figure 2.7 b and d), appearing similarly as an armchair edge, because of subtle differences in chemical functionality (i.e. mono- vs di-hydrogenation)<sup>73</sup>.

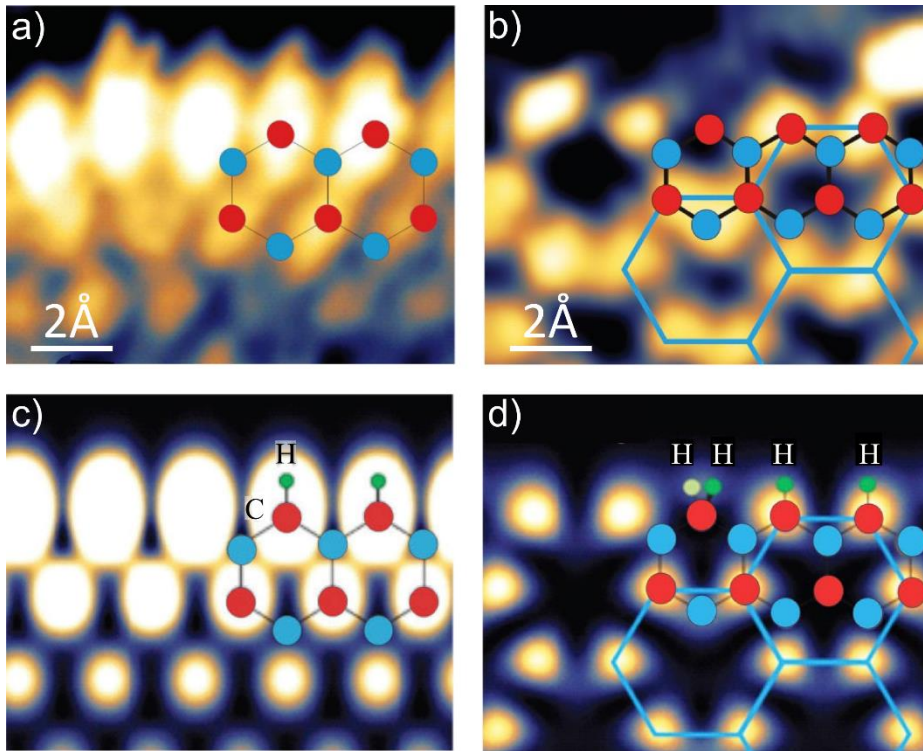


**Figure 2.7.** STM micrograph of mono and di-hydrogenated graphene edges. a) Experimental and b) simulated STM mapping of a zig-zag edge terminated with mono-hydrogenated carbon atoms. c) Experimental and d) simulated STM mapping of a zig-zag edge presenting mixed mono and di-hydrogenated carbon atoms. The small hexagonal unit cells represent the structure of graphene, while the large ones indicate the superlattice due to the underlying graphitic substrate. The presence of a di-hydrogenated carbon atom on the edge can locally destroy the edge state typical of a zig-zag edge configuration, resulting in a dark spot on the STM micrograph<sup>73</sup>.

Not only the geometrical shape of graphene edges tunes the electronic characteristics of graphene edges, but also the finest chemistry of the edges, which can be probed by means of STM imaging, at the cost of systematic DFT calculations.

### 2.5.2 X-ray photoelectron spectroscopy, XPS

X-ray photoelectron spectroscopy (XPS), also referred as ESCA (electron spectroscopy for chemical analysis), is widely used to study the chemical composition of surfaces<sup>108</sup>. An X-ray beam irradiates the surface of the sample and the photons exchange their energy with the electrons of the atoms in proximity of

the surface. The electrons get excited, overwhelming the atomic binding energy and escaping the sample surface. Starting from the kinetic energy of the emitted electrons, it is possible, in principle, to resolve all the elements of the periodic table. Additionally, chemical reactions univocally shift the energy levels of the atoms involved (chemical shifts). Thus, the XPS is suited to read, not only the chemical composition, but even the chemical functionalization of the sample<sup>109</sup>.

Consequently, for each emitted electron, the XPS records an intensity peak at a specific binding energy ( $E_B$ ) which characterizes the elemental composition of the sample. Usually, the X-ray photon source lacks of atomic resolution and the irradiation area can reach several micrometres. Nevertheless, the intensity of the peaks and their shifts, as well as their broadening, can be deconvoluted in order to estimate the relative amount of chemical species on a surface<sup>110</sup>.

Indeed, the peaks deconvolution has been applied to probe the chemical functionalization of graphene edges. Chemically synthesized graphene nanoribbons, which edges were chlorinated, have been analysed by XPS. The chemical synthesis was employed in order to ensure the selective functionalization of the graphene edges. As a result, the C1s peak of the carbon highlights two components: the C=C bond at high intensity, which rises due to the honeycomb lattice of graphene, and a second component induced by the chlorination, Figure 2.8a. Symmetrically, the Cl 2p peak is fully influenced by the bonding with the edge carbon atoms<sup>37</sup>.

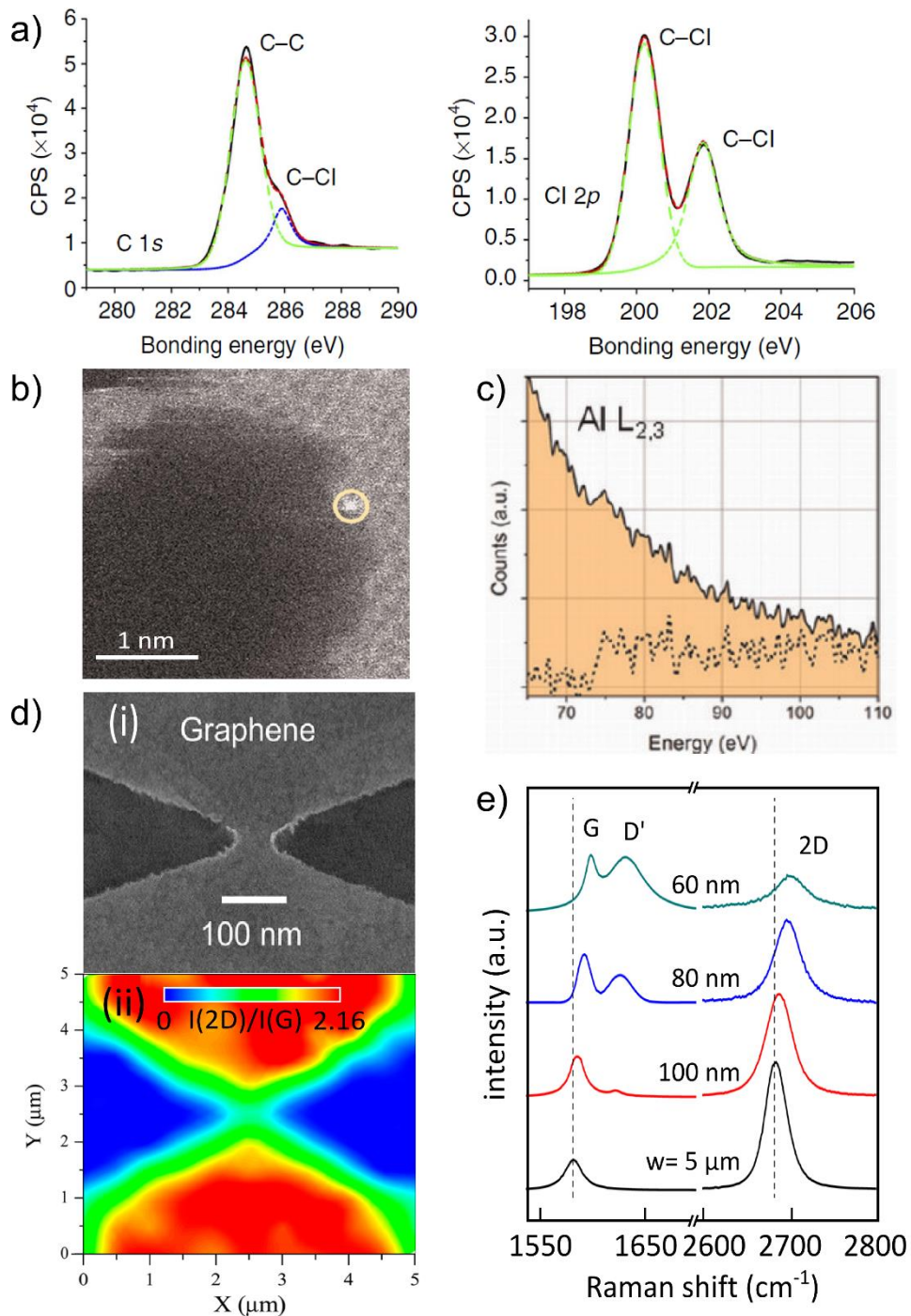


**Figure 2.8.** Spectroscopic characterization of graphene edges. a) X-ray photoelectron spectroscopy of a chlorinated graphene nanoribbon. The C-Cl bond shifts the energy of the C 1s orbital and symmetrically of the Cl 2p energetic levels<sup>37</sup>. b) z-contrast TEM (a mode sensitive to atomic number) image of a sheet of graphene with a large hole. The bright spot marked by the circle corresponds to a single aluminium adatom<sup>18</sup>. c) EELS spectra on the bright spot in b). The dotted line is obtained after filtering and reveals the presence of aluminium<sup>18</sup>. d) Effect of the oxygen plasma etching on the oxidation state of a graphene nanoconstriction. The basal plane of graphene was covered with poly (methyl methacrylate) allowing the etching from the edges. (i) SEM image of the nanoconstriction with a width of 60 nm. (ii) The corresponding I(2D)/I(G) Raman map differentiates the edges from the basal plane, highlighting the oxidation of the edges<sup>10</sup>. e) Raman blue shift of graphene nanoconstriction as a function of the width. The blue-shift is a consequence of the edge oxidation and becomes more prominent in Raman for narrower nanoconstrictions<sup>10</sup>.

Similarly, bromo-phenyl functionalities have been added to the graphene edge using diazonium chemistry. The edge selectivity of the process was demonstrated by the weaker intensity of the C-Br peak of the bromo-phenyl functionalized graphene<sup>45</sup> compared to another graphene sample which surface was chemically modified with the diazonium compound. In fact, the selective edge functionalization offers few binding sites, reducing the intensity of the spectroscopic fingerprint of the functional groups.

### 2.5.3 Electron energy loss spectroscopy, EELS

Electron energy loss spectroscopy (EELS) measures the variation of the kinetic energy of an electron beam once it interacts with the material, probing its chemical composition<sup>111</sup>. Having atomic level resolution, EELS is capable to determine the chemical composition in a specific region of the sample<sup>112</sup>, such as the functionalization of graphene edges.

EELS measurements are performed in a transmission electron microscope, in conjunction with different imaging modes of this instrument. The technique is typically performed on suspended samples in order to avoid the influence of the substrate, even more particularly for graphene, which thickness is order of magnitude shorter than the penetration distances of the electrons.

Experimentally, EELS allows differentiating single atom substitution on graphene. For example, the inelastic scattering induced by the interaction between the electron beam and the graphene highlighted a reduction of the  $\pi^*$  peak energy

passing from the lattice of graphene to the armchair edges and finally to the zig-zag edges<sup>19</sup>.

Additionally, EELS resolved the residual oxidation in multilayer graphene and graphite, where the oxidation of the carbon atoms is tracked by the rise of the k-oxygen peak. The relevance of multilayer systems is correlated to the relaxation mechanisms of the edges in multilayer graphene films. The study underlined the tendency of the edges to close on themselves, limiting the amount of functionalized and reconstructed edges<sup>113</sup>.

Furthermore, EELS resolution is high enough to detect the specific chemistry of unbound impurities such as adatoms (i.e. atoms adsorbed on the graphene surface), if their atomic mass is higher than carbon. Figure 2.8b shows the edge of a graphene sheet close to a large hole obtained by metal mediated etching<sup>18</sup>. The spot marked by the yellow circle appears brighter than the other atoms. This element can be identified in the complementary EELS measurement shown in Figure 2.8c. The presence of a peak around 75 eV in the EELS spectrum is a fingerprint of aluminium (i.e., the metal used for etching the hole in graphene, which got conjugated at the edges of the hole).

#### 2.5.4 Edge functionality probed by Raman spectroscopy

Raman spectroscopy is widely used to characterize both the atomic structure and the electronic properties of graphene<sup>114–116</sup>. Raman resolves the number of graphene layers in few-layers systems<sup>117,118</sup>, and is sensitive to defects and to the presence of edges, more particularly to the atomic arrangement at the edge (i.e. the zig-zag and armchair configuration<sup>119–122</sup>). Raman spectroscopy has also been used to monitor edge disorder, graphene quality, doping and strain<sup>123–127</sup>, as well as to study the chemical functionality of an edge<sup>83</sup>.

The Raman spectrum of graphene shows few characteristic peaks, each corresponding to an inelastic scattering event of the incident light by the lattice of graphene. At an excitation wavelength of 514 nm, the D, G, D' and 2D (also known as G') peaks respectively positioned at  $\sim 1350\text{ cm}^{-1}$ ,  $\sim 1580\text{ cm}^{-1}$ ,  $1620\text{ cm}^{-1}$ ,  $\sim 2700\text{ cm}^{-1}$ , represent the signature of graphene in a Raman spectrum<sup>117,128</sup>. A defect site or an edge breaks the symmetry of the honeycomb lattice and influences the

vibrational modes of the graphene: yielding usually to the rise of the D and D' peaks in the Raman spectrum of graphene<sup>114,115</sup>.

In principle, zig-zag edges inactivate these defect-related peaks<sup>115,118</sup>. Hence, the presence of a D peak can respectively be due to the presence of either zig-zag or armchair edges<sup>119,121</sup>. Nevertheless, the polarization of the incident light, the microscopic disorder of the edges and the size of the illuminated spot area can induce the appearance of a D peak in proximity of a zig-zag edge, limiting the reliability of this particular approach<sup>120</sup>.

The chemical reactivity of graphene can be probed by Raman when the functionalization changes the hybridization of the carbon atoms from  $sp^2$  to  $sp^{348}$ . Before the functionalization, the D peak of graphene presents a strong dependence on the polarization of the incident light, consistent with previous observations and theories<sup>120</sup>. After the functionalization, the polarization dependency is lost. In fact, the re-hybridization introduced by the chemical functionality becomes the main contribution to the D peak. Interestingly, in the case of aryl functionalization of graphene by diazonium chemistry, the ratio  $I(D)/I(G)$  is about two times larger at the edge ( $I(D)/I(G) \sim 0.8$ ) compared to the basal plane ( $I(D)/I(G) \sim 0.4$ ), confirming the higher edge reactivity of graphene<sup>48</sup>.

Another important property of the Raman spectrum of graphene, when studying its functionalization, is the sensitivity of G and 2D peaks to doping (e.g. via oxidation or amination with  $NH_3^{10,83}$ ). A blue and a red shift of the G and 2D peaks occur upon  $p$  and  $n$  type doping respectively (i.e. oxidation and amination). Additionally, the doping leads to a reduction of the intensity of the 2D peak<sup>129</sup>.

Recently, the influence of edge oxidation on the doping of graphene has been studied on nanoconstrictions produced by e-beam lithography and oxygen plasma etching (Figure 2.8d)<sup>10</sup>. The nanoconstriction was fabricated covering the basal plane of graphene with PMMA, while the etching was carried from the edges. The  $I(2D)/I(G)$  mapping of the nanoconstriction (Figure 2.8d (ii)) highlights the decrease of the 2D peak intensity moving from the centre to the edges. Additionally, by reducing the width of nanoconstrictions from 5  $\mu m$  to 60 nm, prominent blue shifts of the G and 2D peaks as well as a strong reduction of the 2D intensity were observed (Figure 2.8e).

The amination of graphene in presence of  $\text{NH}_3$  was followed by mapping the intensity of the D peak and the blue-shift of the G peak<sup>83</sup>. The presence of the D peak reveals that the functionalization under  $\text{NH}_3$  mild plasma conditions occurs preferentially at the edges. This result is consistent with an increased reactivity of the edges compared to the basal plane. Additionally, the chemical doping was further confirmed by the red shift (*n*-type doping) of the G peak.

The Raman technique efficiently provides information about the type of defects formed upon graphene functionalization, but is not capable to identify directly the composition of the chemical groups attached to the reactive sites. Nevertheless, the local variation of the position and intensity of the peaks provides relevant information about, for example, the doping induced by the chemical functionalization of graphene edges.

## 2.6 Summary and outlook

The chemical reactivity of graphene is inherently influenced by its edges. Zig-zag and armchair configurations locally determine the distribution of electrons, and therefore the chemical reactivity of the carbon atoms at the edge sites.

In this context, zig-zag and armchair configurations largely influence the reactivity of the edges towards cycloaddition, condensation, and electrophilic substitution reactions.

Important improvements are required to selectively promote an organic reaction at the edges: at the atomic scale each carbon atom behaves as a reaction site. Each atom is influenced both by its specific properties, such as its chemical functionality, and by the nearby carbon atoms composing the edge. The configuration of the edge (zig-zag or armchair), its position on the edge and the aromaticity of the graphene molecule, all concomitantly determine the reactivity of that particular carbon atom. Consequently, the chemistry of a single carbon atom has hardly been foreseen in the context of further chemical functionalization.

Additionally, STM is very suited to characterize the specific chemistry of a carbon atom on the edge, particularly if combined with DFT calculations. The STM scans the graphene atom by atom acquiring the specific features of the edges, such as

the electron density of states. Alternatively, other characterization methods, such as Raman spectroscopy and XPS are used, although they lack the atomic resolution.

So far, only organic chemistry is capable of offering perfectly tailored graphene edges with a full control over the geometry and the chemistry of the graphene edge. The atomic characterizations of graphene edges, however, remain challenging for many graphene materials systems, where the lack of well suited analytic tools is the obstacle.

## 2.7 References

- (1) Geim, A. K.; Novoselov, K. S. *Nat. Mater.* **2007**, *6*, 183.
- (2) Katsnelson, M. I. *Mater. Today* **2007**, *10* (1), 20–27.
- (3) Wang, L.; Meric, I.; Huang, P. Y.; Gao, Q.; Gao, Y.; Tran, H.; Taniguchi, T.; Watanabe, K.; Campos, L. M.; Muller, D. a; Guo, J.; Kim, P.; Hone, J.; Shepard, K. L.; Dean, C. R. *Science* **2013**, *342* (6158), 614–617.
- (4) Kobayashi, Y.; Fukui, K.; Enoki, T. *Phys. Rev. B* **2006**, *73* (12), 125415.
- (5) Enoki, T.; Fujii, S.; Takai, K. *Carbon* **2012**, *50* (9), 3141–3145.
- (6) Sun, Z.; James, D. K.; Tour, J. M. *J. Phys. Chem. Lett.* **2011**, *2* (19), 2425–2432.
- (7) Gunlycke, D.; Li, J.; Mintmire, J. W.; White, C. T. *Appl. Phys. Lett.* **2007**, *91* (11), 112108.
- (8) Jiang, D.; Sumpter, B. G.; Dai, S. *J. Chem. Phys.* **2007**, *126* (13), 134701.
- (9) Castro Neto, a. H.; Peres, N. M. R.; Novoselov, K. S.; Geim, A. K. *Rev. Mod. Phys.* **2009**, *81* (1), 109–162.
- (10) Iqbal, M. W.; Iqbal, M. Z.; Jin, X.; Hwang, C.; Eom, J. *ACS Appl. Mater. Interfaces* **2014**, *6*, 4207.
- (11) Novoselov, K. S.; Geim, A. K.; Morozov, S. V; Jiang, D.; Zhang, Y.; Dubonos, S. V; Grigorieva, I. V; Firsov, A. A. *Science* **2004**, *306* (5696), 666–669.
- (12) De Arco, L. G.; Zhang, Y.; Kumar, A.; Zhou, C. *IEEE Trans. Nanotechnol.* **2009**, *8* (2), 135–138.
- (13) Böttcher, A.; Heil, M.; Stürzl, N.; Jester, S. S.; Malik, S.; Pérez-Willard, F.; Brenner, P.; Gerthsen, D.; Kappes, M. M. *Nanotechnology* **2006**, *17* (23), 5889–5894.
- (14) Talirz, L.; Söde, H.; Cai, J.; Ruffieux, P.; Blankenburg, S.; Jafaar, R.; Berger, R.; Feng, X.; Müllen, K.; Passerone, D.; Fasel, R.; Pignedoli, C. a; De, H. S.; Ru, P.; Mu, K. *J. Am. Chem. Soc.* **2013**, *135* (6), 2060–2063.
- (15) Eckmann, A.; Felten, A.; Mishchenko, A.; Britnell, L.; Krupke, R.; Novoselov, K. S.; Casiraghi, C. *Nano Lett.* **2012**, *12* (8), 3925–3930.

- (16) Lucchese, M. M.; Stavale, F.; Ferreira, E. H. M.; Vilani, C.; Moutinho, M. V. O.; Capaz, R. B.; Achete, C. a.; Jorio, a. *Carbon* **2010**, *48* (5), 1592–1597.
- (17) Zhang, X.; Yazzev, O. V; Feng, J.; Xie, L.; Tao, C.; Chen, Y.-C.; Jiao, L.; Pedramrazi, Z.; Zettl, A.; Louie, S. G.; Dai, H.; Crommie, M. F. *ACS Nano* **2013**, *7* (1), 198–202.
- (18) Ramasse, Q. Q. M.; Zan, R.; Bangert, U.; Boukhvalov, D. W.; Son, Y.; Novoselov, K. S. *ACS Nano* **2012**, *6* (5), 4063–4071.
- (19) Suenaga, K.; Koshino, M. *Nature* **2010**, *468* (7327), 1088–1090.
- (20) Yazzev, O. V; Capaz, R. B.; Louie, S. G. *J. Phys. Conf. Ser.* **2011**, *302* (1), 012016.
- (21) Sheka, E. F.; Chernozatonskii, L. A. *Int. J. Quantum Chem.* **2009**, *110*(10), 1938-1946.
- (22) Cervantes-Sodi, F.; Csányi, G.; Piskanec, S.; Ferrari, A. C. *Phys. Rev. B* **2008**, *77* (16), 165427.
- (23) Yan, L.; Zheng, Y. B.; Zhao, F.; Li, S.; Gao, X.; Xu, B.; Weiss, P. S.; Zhao, Y. *Chem. Soc. Rev.* **2012**, *41* (1), 97–114.
- (24) He, K.; Lee, G.-D.; Robertson, A. W.; Yoon, E.; Warner, J. H. *Nat. Commun.* **2014**, *5*, 3040.
- (25) Nakada, K.; Fujita, M.; Dresselhaus, G.; Dresselhaus, M. S. M. M. *Phys. Rev. B. Condens. Matter* **1996**, *54* (24), 17954–17961.
- (26) Son, Y.-W.; Cohen, M. L.; Louie, S. G. *Phys. Rev. Lett.* **2006**, *97* (21), 216803.
- (27) Acik, M.; Ā, Y. J. C.; Chabal, Y. J. *Jpn. J. Appl. Phys.* **2011**, *50* (7), 070101.
- (28) Koskinen, P.; Malola, S.; Häkkinen, H. *Phys. Rev. B* **2009**, *80* (7), 073401.
- (29) Wassmann, T.; Seitsonen, A. P.; Saitta, A. M.; Lazzeri, M.; Mauri, F. *J. Am. Chem. Soc.* **2010**, *132* (10), 3440–3451.
- (30) Baldoni, M.; Sgamellotti, A.; Mercuri, F. *Chem. Phys. Lett.* **2008**, *464* (4–6), 202–207.
- (31) Fujii, S.; Enoki, T. *Acc. Chem. Res.* **2013**, *46* (10), 2202–2210.
- (32) Jiang, D.; Chen, Z. *Graphene Chemistry: Theoretical Perspectives*; Wiley,

**2013.**

- (33) Wassmann, T.; Seitsonen, A.; Saitta, a.; Lazzeri, M.; Mauri, F. *Phys. Rev. Lett.* **2008**, *101* (9), 096402.
- (34) Seitsonen, A. P.; Saitta, a. M.; Wassmann, T.; Lazzeri, M.; Mauri, F. *Phys. Rev. B* **2010**, *82* (11), 115425.
- (35) Kariuki, J. K.; McDermott, M. T. *Langmuir* **1999**, *15* (19), 6534–6540.
- (36) Quintana, M.; Montellano, A.; del Rio Castillo, A. E.; Van Tendeloo, G.; Bittencourt, C.; Prato, M. *Chem. Commun.* **2011**, *47* (33), 9330–9332.
- (37) Tan, Y.-Z.; Yang, B.; Parvez, K.; Narita, A.; Osella, S.; Beljonne, D.; Feng, X.; Müllen, K. *Nat. Commun.* **2013**, *4*, 2646.
- (38) Lu, Y.; Lerner, M. B.; John Qi, Z.; Mitala, J. J.; Hsien Lim, J.; Discher, B. M.; Charlie Johnson, A. T. *Appl. Phys. Lett.* **2012**, *100* (3), 033110.
- (39) Chua, C. K.; Pumera, M. *Chem. Soc. Rev.* **2013**, *42* (8), 3222–3233.
- (40) Liu, K.; Chen, S.; Luo, Y.; Jia, D.; Gao, H.; Hu, G.; Liu, L. *Compos. Sci. Technol.* **2013**, *88*, 84–91.
- (41) Jeon, I.-Y.; Choi, E.-K.; Bae, S.-Y.; Baek, J.-B. *Nanoscale Res. Lett.* **2010**, *5* (10), 1686–1691.
- (42) Zhao, W.; Fang, M.; Wu, F.; Wu, H.; Wang, L.; Chen, G. *J. Mater. Chem.* **2010**, *20* (28), 5817.
- (43) Jeon, I.-Y.; Choi, H.-J.; Jung, S.-M.; Seo, J.-M.; Kim, M.-J.; Dai, L.; Baek, J.-B. *J. Am. Chem. Soc.* **2013**, *135* (4), 1386–1393.
- (44) Xu, J.; Shui, J.; Wang, J.; Wang, M.; Liu, H.-K.; Dou, S. X.; Jeon, I.-Y.; Seo, J.-M.; Baek, J.-B.; Dai, L. *ACS Nano* **2014**, *8* (10), 10920–10930.
- (45) Sun, Z.; Kohama, S.; Zhang, Z.; Lomeda, J. R.; Tour, J. M. *Nano Res.* **2010**, *3* (2), 117–125.
- (46) Kariuki, J. K.; McDermott, M. T. *Langmuir* **2001**, *17* (19), 5947–5951.
- (47) Park, J.; Yan, M. *Acc. Chem. Res.* **2012**, *46* (1), 181–189.
- (48) Sharma, R.; Baik, J. H.; Perera, C. J.; Strano, M. S. *Nano Lett.* **2010**, *10* (2), 398–405.

- (49) Paulus, G. L. C.; Wang, Q. H.; Strano, M. S. *Acc. Chem. Res.* **2013**, *46* (1), 160–170.
- (50) Jeon, I.-Y.; Shin, Y.-R.; Sohn, G.-J.; Choi, H.-J.; Bae, S.-Y.; Mahmood, J.; Jung, S.-M.; Seo, J.-M.; Kim, M.-J.; Wook Chang, D.; Dai, L.; Baek, J.-B. *Proc. Natl. Acad. Sci. U. S. A.* **2012**, *109* (15), 5588–5593.
- (51) Chen, L.; Hernandez, Y.; Feng, X.; Müllen, K. *Angew. Chem. Int. Ed. Engl.* **2012**, *51* (31), 7640–7654.
- (52) Smith, B. W.; Luzzi, D. E. *J. Appl. Phys.* **2001**, *90* (7), 3509.
- (53) Girit, C. O.; Meyer, J. C.; Erni, R.; Rossell, M. D.; Kisielowski, C.; Yang, L.; Park, C.-H.; Crommie, M. F.; Cohen, M. L.; Louie, S. G.; Zettl, A. *Science*. **2009**, *323* (5922), 1705–1708.
- (54) Schneider, F.; Houben, L.; Malladi, S. K.; Dekker, C.; Xu, Q.; Wu, M.-Y.; Schneider, G. F.; Houben, L.; Malladi, S. K.; Dekker, C.; Yucelen, E.; Dunin-Borkowski, R. E.; Zandbergen, H. W. *ACS Nano* **2013**, *7* (2), 1566–1572.
- (55) Schneider, G. F.; Kowalczyk, S. W.; Calado, V. E.; Pandraud, G.; Zandbergen, H. W.; Vandersypen, L. M. K.; Dekker, C. *Nano Lett.* **2010**, *10* (8), 3163–3167.
- (56) Lee, G.; Cho, K. *Phys. Rev. B* **2009**, *79* (16), 165440.
- (57) Wang, Z.; Li, Q.; Zheng, H.; Ren, H.; Su, H.; Shi, Q.; Chen, J. *Phys. Rev. B* **2007**, *75* (11), 113406.
- (58) Terrones, H.; Lv, R.; Terrones, M.; Dresselhaus, M. S. *Rep. Prog. Phys.* **2012**, *75* (6), 062501.
- (59) Qi, Z. J.; Rodríguez-Manzo, J. a; Botello-Méndez, A. R.; Hong, S. J.; Stach, E. a; Park, Y. W.; Charlier, J.-C.; Drndić, M.; Johnson, a T. C. *Nano Lett.*, **2014**, *14* (8), pp 4238–4244.
- (60) Fischbein, M. D.; Drndić, M. *Appl. Phys. Lett.* **2008**, *93* (11), 113107.
- (61) Merchant, C. A.; Healy, K.; Wanunu, M.; Ray, V.; Peterman, N.; Bartel, J.; Fischbein, M. D.; Venta, K.; Luo, Z.; Johnson, A. T. C.; Drndić, M.; et al. *Nano Lett.* **2010**, *10* (8), 2915–2921.
- (62) Garaj, S.; Hubbard, W.; Reina, A.; Kong, J.; Branton, D.; Golovchenko, J. a. *Nature* **2010**, *467* (7312), 190–193.

- (63) Traversi, F.; Raillon, C.; Benameur, S. M.; Liu, K.; Khlybov, S.; Tosun, M.; Krasnozhan, D.; Kis, A.; Radenovic, A. *Nat. Nanotechnol.* **2013**, *8* (12), 939–945.
- (64) Liu, K.; Feng, J.; Kis, A.; Radenovic, A. *ACS Nano* **2014**, *8* (3), 2504–2511.
- (65) Liu, S.; Lu, B.; Zhao, Q.; Li, J.; Gao, T.; Chen, Y.; Zhang, Y.; Liu, Z.; Fan, Z.; Yang, F.; You, L.; Yu, D. *Adv. Mater.* **2013**, *25*, 4549–4554.
- (66) Song, B.; Schneider, G. F.; Xu, Q.; Pandraud, G.; Dekker, C.; Zandbergen, H. *Nano Lett.* **2011**, *11* (6), 2247–2250.
- (67) Bell, D. C.; Lemme, M. C.; Stern, L. a; Williams, J. R.; Marcus, C. M. *Nanotechnology* **2009**, *20* (45), 455301.
- (68) Ward, B. W.; Notte, J. a.; Economou, N. P. *J. Vac. Sci. Technol. B Microelectron. Nanom. Struct.* **2006**, *24* (6), 2871.
- (69) Xie, L.; Jiao, L.; Dai, H. *J. Am. Chem. Soc.* **2010**, *132* (42), 14751–14753.
- (70) Wang, X.; Dai, H. *Nat. Chem.* **2010**, *2* (8), 661–665.
- (71) Jia, X.; Campos-Delgado, J.; Terrones, M.; Meunier, V.; Dresselhaus, M. S. *Nanoscale* **2011**, *3* (1), 86–95.
- (72) Kobayashi, Y.; Fukui, K.; Enoki, T.; Kusakabe, K.; Kaburagi, Y. *Phys. Rev. B* **2005**, *71* (19), 193406.
- (73) Ziatdinov, M.; Fujii, S.; Kusakabe, K.; Kiguchi, M.; Mori, T.; Enoki, T. *Phys. Rev. B* **2013**, *87* (11), 115427.
- (74) Lu, Y. H.; Wu, R. Q.; Shen, L.; Yang, M.; Sha, Z. D.; Cai, Y. Q.; He, P. M.; Feng, Y. P. *Appl. Phys. Lett.* **2009**, *94* (12), 122111.
- (75) Wagner, P.; Ivanovskaya, V. V.; Melle-Franco, M.; Humbert, B.; Adjizian, J.-J.; Briddon, P. R.; Ewels, C. P. *Phys. Rev. B* **2013**, *88* (9), 094106.
- (76) Simbeck, A. J.; Gu, D.; Kharche, N.; Satyam, P. V.; Avouris, P.; Nayak, S. K. *Phys. Rev. B* **2013**, *88* (3), 035413.
- (77) Ohtsuka, M.; Fujii, S.; Kiguchi, M.; Enoki, T. *ACS Nano* **2013**, *7* (8), 6868–6874.
- (78) Hod, O.; Barone, V.; Peralta, J. E.; Scuseria, G. E. *Nano Lett.* **2007**, *7* (8),

2295–2299.

- (79) Yang, X.; Dou, X.; Rouhanipour, A.; Zhi, L.; Räder, H. J.; Müllen, K.; Ra, H. J.; Mu, K. *J. Am. Chem. Soc.* **2008**, *130* (13), 4216–4217.
- (80) Cai, J.; Ruffieux, P.; Jaafar, R.; Bieri, M.; Braun, T.; Blankenburg, S.; Fasel, R.; Muoth, M.; Seitsonen, A. P.; Saleh, M.; Feng, X.; Mu, K.; Müllen, K. *Nature* **2010**, *466* (7305), 470–473.
- (81) Baraket, M.; Stine, R.; Lee, W. K.; Robinson, J. T.; Tamanaha, C. R.; Sheehan, P. E.; Walton, S. G. *Appl. Phys. Lett.* **2012**, *100* (23), 233123.
- (82) Wang, X.; Li, X.; Zhang, L.; Yoon, Y.; Weber, P. K.; Wang, H.; Guo, J.; Dai, H. *Science* **2009**, *324* (5928), 768–771.
- (83) Kato, T.; Jiao, L.; Wang, X.; Wang, H.; Li, X.; Zhang, L.; Hatakeyama, R.; Dai, H. *Small* **2011**, *7* (5), 574–577.
- (84) Vo, T. H.; Shekhirev, M.; Kunkel, D. A.; Morton, M. D.; Berglund, E.; Kong, L.; Wilson, P. M.; Dowben, P. A.; Enders, A.; Sinitskii, A. *Nat. Commun.* **2014**, *5*, 3189.
- (85) Li, X.; Cai, W.; An, J.; Kim, S.; Nah, J.; Yang, D.; Piner, R.; Velamakanni, A.; Jung, I.; Tutuc, E.; Banerjee, S. K.; Colombo, L.; Ruoff, R. S. *Science*. **2009**, *324* (5932), 1312–1314.
- (86) Biró, L. P.; Lambin, P. *Carbon* **2010**, *48* (10), 2677–2689.
- (87) Puddy, R. K.; Scard, P. H.; Tyndall, D.; Connolly, M. R.; Smith, C. G.; Jones, G. A. C.; Lombardo, A.; Ferrari, A. C.; Buitelaar, M. R. *Appl. Phys. Lett.* **2011**, *98* (13), 133120.
- (88) Hiura, H. *Appl. Surf. Sci.* **2004**, *222* (1–4), 374–381.
- (89) Park, J.; Kim, K. B.; Park, J.-Y.; Choi, T.; Seo, Y. *Nanotechnology* **2011**, *22* (33), 335304.
- (90) Kondo, S.; Lutwyche, M.; Wada, Y. *Appl. Surf. Sci.* **1994**, *75* (1–4), 39–44.
- (91) Albrecht, T. R.; Dovek, M. M.; Kirk, M. D.; Lang, C. A.; Quate, C. F.; Smith, D. P. E. *Appl. Phys. Lett.* **1989**, *55* (17), 1727.
- (92) Kurra, N.; Prakash, G.; Basavaraja, S.; Fisher, T. S.; Kulkarni, G. U.; Reifengerger, R. G. *Nanotechnology* **2011**, *22* (24), 245302.

- (93) Masubuchi, S.; Ono, M.; Yoshida, K.; Hirakawa, K.; Machida, T. *Appl. Phys. Lett.* **2009**, *94* (8), 082107.
- (94) Nemes-Incze, P.; Tapasztó, L.; Magda, G. Z.; Osváth, Z.; Dobrik, G.; Jin, X.; Hwang, C.; Biró, L. P. *Appl. Surf. Sci.* **2014**, *291*, 48–52.
- (95) Weng, L.; Zhang, L.; Chen, Y. P.; Rokhinson, L. P. *Appl. Phys. Lett.* **2008**, *93* (9), 093107.
- (96) Pumera, M. *Chem. Soc. Rev.* **2010**, *39* (11), 4146.
- (97) Ambrosi, A.; Bonanni, A.; Pumera, M. *Nanoscale* **2011**, *3* (5), 2256–2260.
- (98) Yuan, W.; Zhou, Y.; Li, Y.; Li, C.; Peng, H.; Zhang, J.; Liu, Z.; Dai, L.; Shi, G. *Sci. Rep.* **2013**, *3* (1), 2248.
- (99) Banerjee, S.; Shim, Â. J.; Rivera, Â. J.; Jin, X.; Estrada, D.; Solovyeva, V.; Shim, J.; Rivera, J.; You, X.; Pak, J.; Pop, E.; Aluru, N.; Bashir, R. *ACS Nano* **2013**, *7* (1), 834–843.
- (100) Brownson, D. A. C.; Kampouris, D. K.; Banks, C. E. *Chem. Soc. Rev.* **2012**, *41* (21), 6944–6976.
- (101) McCreery, R. L.; McDermott, M. T. *Anal. Chem.* **2012**, *84* (5), 2602–2605.
- (102) Shang, N. G.; Papakonstantinou, P.; McMullan, M.; Chu, M.; Stamboulis, A.; Potenza, A.; Dhesi, S. S.; Marchetto, H. *Adv. Funct. Mater.* **2008**, *18* (21), 3506.
- (103) Akhavan, O.; Ghaderi, E.; Rahighi, R. *ACS Nano* **2012**, *6* (4), 2904–2916.
- (104) Ambrosi, A.; Bonanni, A.; Sofer, Z.; Cross, J. S.; Pumera, M. *Chemistry* **2011**, *17* (38), 10763–10770.
- (105) Zhou, M.; Zhai, Y.; Dong, S. *Anal. Chem.* **2009**, *81* (14), 5603.
- (106) Klusek, Z.; Waqar, Z.; Denisov, E. .; Kompaniets, T. .; Makarenko, I. .; Titkov, a. .; Bhatti, A. . *Appl. Surf. Sci.* **2000**, *161* (3–4), 508–514.
- (107) Tao, C.; Jiao, L.; Yazyev, O. V.; Chen, Y.-C.; Feng, J.; Zhang, X.; Capaz, R. B.; Tour, J. M.; Zettl, A.; Louie, S. G.; Dai, H.; Crommie, M. F. *Nat. Phys.* **2011**, *7* (8), 616–620.
- (108) Turner, N. H. *Anal. Chem.* **1988**, *60* (12), 377–387.

- (109) Henning, B.; Holger, J. *Surface and Thin Film Analysis: A Compendium of Principles, Instrumentation, and Applications*; John Wiley & Sons, **2011**.
- (110) Kuwana, T. *Physical Methods in Modern Chemical Analysis, Volume 2*; Elsevier Science, **2012**.
- (111) Egerton, R. F. *Reports Prog. Phys.* **2009**, *72* (1), 016502.
- (112) Suenaga, K.; Tence, M.; Mory, C.; Colliex, C.; Kato, H.; Okazaki, T.; Shinohara, H.; Hirahara, K.; Bandow, S.; Iijima, S. *Science* **2000**, *290* (5500), 2280–2282.
- (113) Liu, Z.; Suenaga, K.; Harris, P.; Iijima, S. *Phys. Rev. Lett.* **2009**, *102* (1), 015501.
- (114) Malard, L. M.; Pimenta, M. a.; Dresselhaus, G.; Dresselhaus, M. S. *Phys. Rep.* **2009**, *473* (5–6), 51–87.
- (115) Ferrari, A. C.; Basko, D. M. *Nat. Nanotechnol.* **2013**, *8* (4), 235–246.
- (116) Zhang, D.; Yang, J.; Li, Y. *Small* **2013**, *9* (8), 1284–1304.
- (117) Ferrari, A. C.; Meyer, J. C.; Scardaci, V.; Casiraghi, C.; Lazzeri, M.; Mauri, F.; Piscanec, S.; Jiang, D.; Novoselov, K. S.; Roth, S.; Geim, A. K. *Phys. Rev. Lett.* **2006**, *97* (18), 187401.
- (118) Cançado, L.; Reina, a.; Kong, J.; Dresselhaus, M. M.; Cancado, L. *Phys. Rev. B* **2008**, *77* (24), 245408.
- (119) You, Y.; Ni, Z.; Yu, T.; Shen, Z. *Appl. Phys. Lett.* **2008**, *93* (16), 163112.
- (120) Casiraghi, C.; Hartschuh, A.; Qian, H.; Piscanec, S.; Georgi, C.; Fasoli, A.; Novoselov, K. S.; Basko, D. M.; Ferrari, A. C. *Nano Lett.* **2009**, *9* (4), 1433–1441.
- (121) Xu, Y. N.; Zhan, D.; Liu, L.; Suo, H.; Ni, Z. H.; Nguyen, T. T.; Zhao, C.; Shen, Z. X. *ACS Nano* **2011**, *5* (1), 147–152.
- (122) Begliarbakov, M.; Sul, O.; Kalliakos, S.; Yang, E.-H.; Strauf, S. *Appl. Phys. Lett.* **2010**, *97* (3), 031908.
- (123) Ferrari, A. C. *Solid State Commun.* **2007**, *143* (1–2), 47–57.
- (124) Ferrari, A. C.; Robertson, J. *Phys. Rev. B* **2000**, *61* (20), 14095–14107.
- (125) Venezuela, P.; Lazzeri, M.; Mauri, F. *Phys. Rev. B* **2011**, *84* (3), 035433.

- (126) Stampfer, C.; Molitor, F.; Graf, D.; Ensslin, K.; Jungen, A.; Hierold, C.; Wirtz, L. *Appl. Phys. Lett.* **2007**, *91* (24), 241907.
- (127) Xie, W.-G. W.; Lai, X.; Wang, X.-M. X.; Wan, X.; Yan, M.-L.; Mai, W.-J.; Liu, P.-Y.; Chen, J.; Xu, J. *Spectrosc. Lett.* **2014**, *47* (6), 465–470.
- (128) Jorio, A. *ISRN Nanotechnol.* **2012**, *2012* (2), 1–16.
- (129) Kalbac, M.; Reina-cecco, A.; Farhat, H.; Kong, J.; Kavan, L.; Dresselhaus, M. S. *ACS Nano* **2010**, *4* (10), 6055–6063.